Journal of Materials Chemistry C

ROYAL SOCIETY OF CHEMISTRY

PAPER

View Article Online
View Journal | View Issue

Cite this: J. Mater. Chem. C, 2022, 10, 6009

Modulating electronic and optical properties of monolayered MoS_2 by covalent mono- and bisfunctionalization†

Kangli Wang, * Marco Kapitzke, Lauren Green and Beate Paulus

By employing first-principles simulations, we present theoretical predictions regarding the modification of structural, electronic and optical properties of 2H- and 1T′-MoS_2 monolayers by covalent mono- and bisfunctionalization. Specifically, non-aromatic groups (–F, $–NH_2$, $–CH_3$, $–CH_2CH_2$ CN and $–CH_2CH_2$ OH) and aromatic (–Ph, $–PhNO_2$ and PhOH) groups are utilized for monofunctionalization, and –F/$–NH_2$, $–NH_2/–CH_3$ and $–CH_3$/–Ph for bisfunctionalization. The stability of functionalized 2H- and 1T′-MoS_2 monolayers mainly depends on the bonded groups and their surface coverage. In particular, the mixed bisfunctionalization with –F/$–CH_3$ and $–NH_2/–CH_3$ groups enhances the stability of 2H-MoS_2 through the formation of intermolecular hydrogen bonds. Both 2H- and 1T′-MoS_2 can serve not only as electron donors, but also as electron acceptors, subject to the charge transfer behavior of the attached groups. Furthermore, mono- and bisfunctionalization are predicted to be efficient approaches to control the electronic band gaps in 2H- and 1T′-MoS_2, where the corresponding values can be tuned by varying the coverage of the absorbed groups. At the same time, the choice of the chemical groups and their coverage also effectively determines the optical adsorption range and intensity. Therefore, our work shows that chemical functionalization of 2D materials with varying coverage can be an important approach to extend the scope of 2D materials in specific electronic and optoelectronic applications.

Received 27th January 2022,
Accepted 18th March 2022

DOI: 10.1039/d2tc00391k

rsc.li/materials-c

1 Introduction

Monolayered MoS_2 is one of the most common transition metal dichalcogenides (TMDCs) and finds a range of promising applications such as photodetectors,[1–3] advanced catalysts,[4,5] gas sensors,[6,7] batteries[8,9] and solar cells[10,11] due to its unique features and excellent tunability of the electronic properties. Depending on the arrangement of S atoms on both sides of Mo atoms, the MoS_2 monolayer has one of the three polytypic structures: the 2H, 1T and 1T′ (distorted 1T) phases.[12–15] The Mo atom in the 2H and 1T phases is coordinated by six S atoms in an octahedral and trigonal prismatic arrangement, respectively. Generally, 1T phase is unstable under free-standing conditions and can be easily converted into the meta stable 1T′ phase that consists of zigzag Mo chains. Owing to the different localization behaviors of the d-band in Mo,[16] 2H-MoS_2 is a semiconductor with a sizeable band gap and a photoluminophore, whereas 1T-MoS_2 exhibits metallic character without photoluminescence.[1,2,14–16] Interestingly, the 1T and 2H phases can also coexist in the same MoS_2 monolayer,[17] thereby allowing low contact resistance and holding high catalytic activity.[18,19]

To further improve the applicability of TMDCs in diverse fields, many methods have been developed to tune their properties, such as adsorption of gas molecules[20–22] and strain engineering.[23,24] Among them, covalent functionalization offers the most compelling route. Since the basal plane of 1T-MoS_2 is sensitive to functionalization, chemically exfoliated MoS_2 can react with phenyl diazonium salts[25,26] or organohalides (–I or –Br)[27,28] to form new S–Mo bonds. Although 2H-MoS_2 has a relatively inert basal plane, it is reported to be covalently functionalized by bonding through sulfur defects,[29–31] coordinating to metal complexes,[32] reacting with aryl diazonium[33] and thiolate salts[34] as well as maleimide derivatives.[35] More impressively, a bisfunctionalized MoS_2 hybrid structure bearing both alkyl and aryl groups has been recently demonstrated.[36] On the other hand, the coverage of functional groups achieved after functionalization varies from 10% to 70%, depending on different methods and conditions.[25,27,33,36,37] Given these experimental results, a theoretical perspective on how covalent functionalization alters the electronic and optical properties of 2H- and 1T-MoS_2 (or 1T′-MoS_2) is desirable. However, previous computational

Institut für Chemie und Biochemie, Freie Universität Berlin, 14195 Berlin, Germany. E-mail: klwang0329@zedat.fu-berlin.de

† Electronic supplementary information (ESI) available. See DOI: 10.1039/d2tc00391k

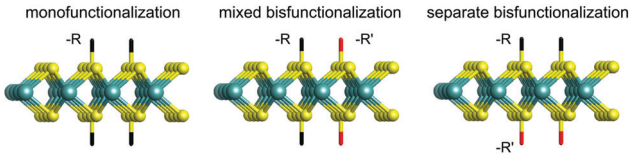

Fig. 1 Schematic representation of mono- and bisfunctionalization considered in this work.

studies mainly focus on the monofunctionalization with small groups (–H, –O, –SH, –NH_2, –CH_3),[38–41] while monofunctionalization with large groups as well as bisfunctionalization is far less explored.[42,43]

In this work, we aim to give a comprehensive understanding towards the two-sided covalent functionalization of monolayered 2H- and 1T′-MoS_2. We do not consider the functionalized T phase as this structure evolves to the T′ phase upon structural optimization. Non-aromatic groups (–F, –NH_2, –CH_3, –CH_2CH_2 CN and –CH_2CH_2 OH) and aromatic groups (–Ph, –$PhNO_2$ and PhOH) are applied to monofunctionalize 2H- and 1T′-MoS_2. Furthermore, bisfunctionalization of MoS_2 is also considered in this study, including mixed bisfunctionalization (m-F/–NH_2, m-NH_2/–CH_3 and m-CH_3/–Ph) where each group is bonded to both sides of the MoS_2 monolayer and separate bisfunctionalization (s-F/–NH_2, s-NH_2/–CH_3 and s-CH_3/–Ph) where each side of the monolayer is uniquely functionalized by a specie as illustrated in Fig. 1. It is well known that density functional theory (DFT) alone is ill-equipped to describe the electronic band structure, especially when predicting the size of the band gap for semiconductors or insulators. To accurately model the electronic band structure and optical absorption, we employ the GW (Green's function (G) and screened Coulomb (W) potential) approximation within the framework of many-body perturbation theory and Bethe–Salpeter equation based on the DFT method (DFT-GW-BSE).[44–47] This method includes self-energy and excitonic effects, and thus has been successfully applied to a wide variety of materials.[48–51]

2 Computational details

All of the calculations are performed with the GPAW code.[52] The structure is relaxed until all forces are below 0.01 eV $Å^{-1}$ using the Perdew–Burke–Ernzerhof (PBE) exchange–correlation functional[53] with 450 eV plane wave cutoff, and more than 15 Å between periodically repeated layers. A 4 × 4 supercell (contains 32 adsorption sites) is considered to bond with 2, 4,. . ., 14 groups corresponding to the functionalized coverages varying from 6.25% to 43.75%; a 2 × 2 supercell with 2 groups corresponds to a 50% coverage. A Γ-centered Monkhorst–Pack k-grid scheme of 6 × 6 × 1 and 12 × 12 × 1 are used for 4 × 4 and 2 × 2 supercells, respectively. The charge transfer between the group and the substrate is discussed by means of Bader analysis.[54]

The DFT-GW-BSE calculations are performed according to following protocol. Firstly, standard Kohn–Sham DFT calculations are performed to obtain the ground state Kohn–Sham orbitals. The same parameters as for the structural relaxation calculations are adopted. Then, non-self-consistent G_0W_0 is employed to calculate the quasiparticle (QP) band structures, which involves the calculation of QP energy using the input DFT orbitals. To avoid spurious interactions between neighboring supercells, a 2D Coulomb truncation is applied with 8 Å vacuum ensuring the convergence of the QP band gap. The dielectric matrix and correlation self-energy is evaluated using a cutoff of 50 eV on a nonlinear grid with $\Delta\omega_0 = 0.25$ eV frequency spacing. At $\omega_2 = 10$ eV, this spacing increases to $2\Delta\omega_0$. Finally, the BSE spectrum is obtained by applying the Tamm–Dancoff approximation.[55,56] The 24 highest valence and 48 lowest conduction bands are utilized as a basis for excitonic eigenstates, which is enough to attain converged optical absorption spectrum. A Lorentzian broadening of 0.05 eV is employed for all the optical calculations. The convergence tests for the DFT-GW-BSE treatment are in ESI† (see Fig. S1, ESI†).

3 Results and discussion

Average binding energy

We first employ DFT to determine the most favorable adsorption sites and calculate the thermodynamic stability of the functionalized MoS_2 monolayer by computing the average binding energy per group as a function of the adsorbate coverages:

$$\Delta E = (E_{tot} - E_{MoS_2} - nE_{group})/n, \quad (1)$$

where E_{tot} is the total energy of functionalized MoS_2, E_{MoS_2} is the energy of the pristine 2H- or 1T′-MoS_2 monolayer, E_{group} is the energy of the isolated group and n is the number of groups that are added. A more negative binding energy indicates a stronger preference of the structure, while a positive value of the binding energy implies an unstable structure. The optimized structures for monofunctionalized MoS_2 at 6.25% coverage and bisfunctionalized MoS_2 at 12.5% coverage are presented in Fig. 2. The obtained average binding energies as a function of coverages are plotted in Fig. 3. As depicted in Fig. 3(a) and (c), at low coverage up to 25%, the average binding energy of each group on the functionalized 2H-MoS_2 system slightly decrease with the increase of coverage for most of the studied functionalizations. This indicates that the adsorbed group can act as an anchor, boosting further functionalization of 2H-MoS_2. When the coverage exceeds 25%, the computed binding energies of all systems become more positive as the coverage grows, suggesting that high coverage of 2H-MoS_2 is unfavorable due to the repulsive interaction between the adsorbed species. At high coverage, the 2H phase functionalized by –NH_2 and s-NH_3/–CH_3 tends to release NH_3 gas and therefore a stable covalent functionalization of 2H phase is not possible. However, mixed bisfunctionalization can promote the formation of intermolecular hydrogen bonds and thereby improves their stability as the coverage increases, such as m-F/–CH_3 and m-NH_2/–CH_3. In comparison to other groups, the average binding energy of –CH_2CH_2 CN and –CH_2CH_2 OH on

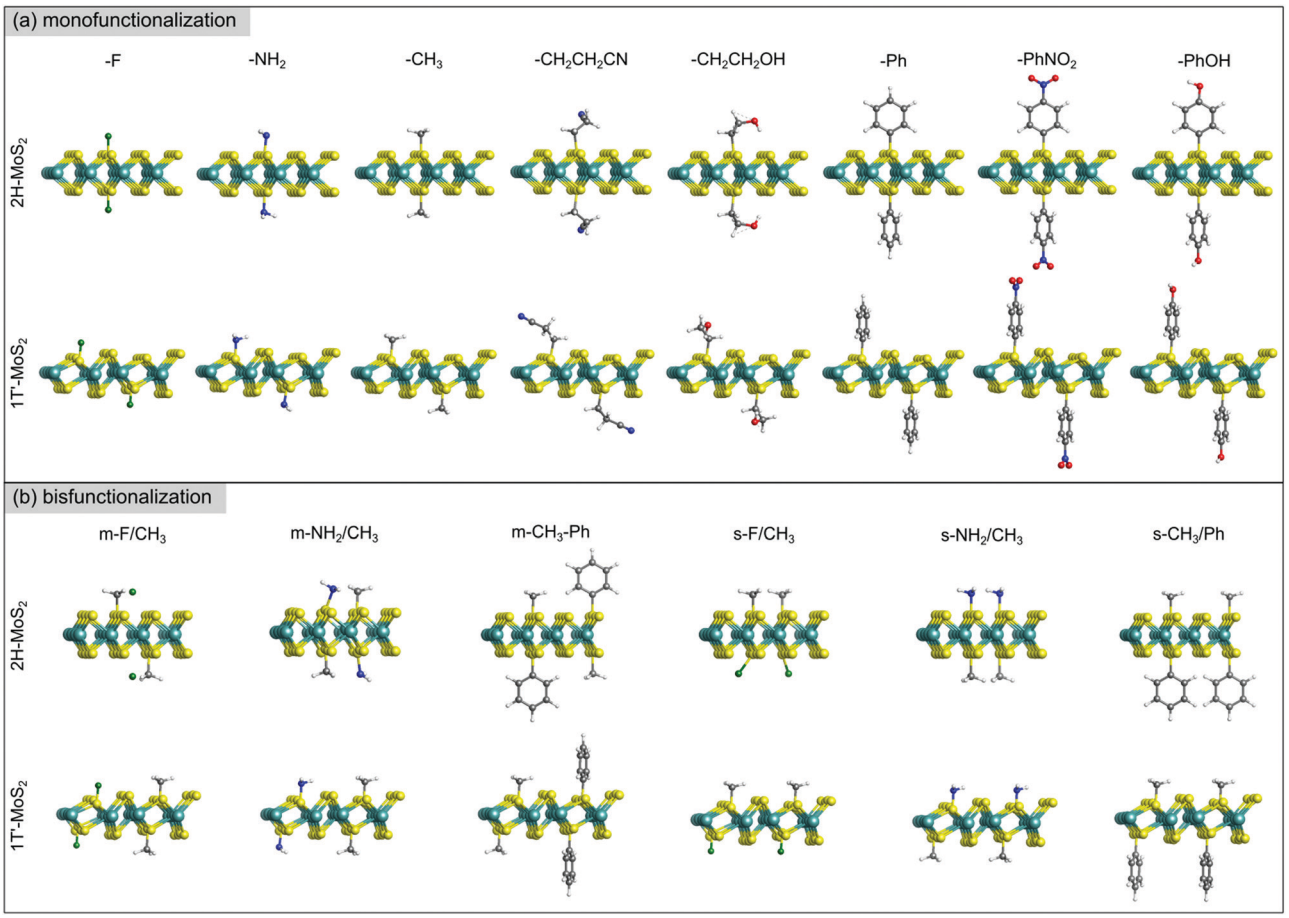

Fig. 2 Ball-and-stick model of the optimized structures of the monofunctionalized (6.25% coverage) and bisfunctionalized (12.5% coverage) 2H- and 1T′-MoS_2 by different groups (side and perspective views). The hydrogen, carbon, nitrogen, oxygen, fluorine, sulfur and molybdenum are in color white, gray, blue, red, green, yellow and turquoise, respectively.

the basal surface of 2H-MoS_2 is rather more positive and the Mo–C bond length is more than 1.91 Å. This is attributed to the stereostructures of $-CH_2CH_2$ CN and $-CH_2CH_2$ OH that weaken the interaction between the chemical adsorbate and 2H-MoS_2.

Fig. 3(b) and (d) illustrate the average binding energy of the functionalized 1T′-MoS_2 at varying coverage. For the 1T′ phase, the average binding energy of each system reaches a minimum at 12.5% coverage, which is smaller than that of 2H-MoS_2. Furthermore, a considerable stability range of the functionalized 1T′ phase can be noticed, exhibiting a negative average binding energy even at 50% coverage. This suggests the possibility of high functional group coverage of functionalized 1T′-MoS_2, which is consistent with previous experimental observations.[37] In addition, the average binding energy of 1T′-MoS_2 is much smaller than that of 2H-MoS_2 for any given coverage, indicating that the reaction of chemical functionalization of the 1T′ phase is thermodynamically more favorable. This is attributed to the well-paired electrons in 2H-MoS_2, whereas the electronic states around the Fermi level are only partially filled in 1T′-MoS_2.[39]

By comparing the total energy between 2H- and 1T′-MoS_2, we investigate the phase stability (see Fig. S3, ESI†). At low coverage, the functionalized 2H phase is more energetically stable regardless of mono- or bisfunctionalization. As the coverage increases, the energy difference becomes smaller. In particular, at high coverage, the functionalized 1T′ phase is more stable than 2H case. This indicates that the selective tuning of the coverage of covalent functionalization enables the phase transformation of MoS_2.

To gain an insight into the bonding nature of the considered systems, we further execute the Bader charge analysis to investigate the charge transfer between the MoS_2 monolayer and the attached groups. The corresponding results are displayed in Fig. S4 (ESI†). When –F, $-NH_2$, m-F/$-CH_3$ and s-F/$-CH_3$ are bonded to the surface of both 2H- and 1T′-MoS_2, the electron is transferred to the groups from the substrate which acts as an electron-donor. In contrast, an inverted electron flow can be recognized for other functional groups, for instance $-CH_3$, $-CH_2CH_2$ CN, $-CH_2CH_2$ OH, –Ph, $-PhNO_2$ and –PhOH. Here the substrate gains electrons despite bare MoS_2 is an n-type semiconductor. The direction of charge transfer exhibits a clear dependence on the electron donating or withdrawing ability of the adsorbed species. Correlation of the binding energy with the electron donating or withdrawing properties

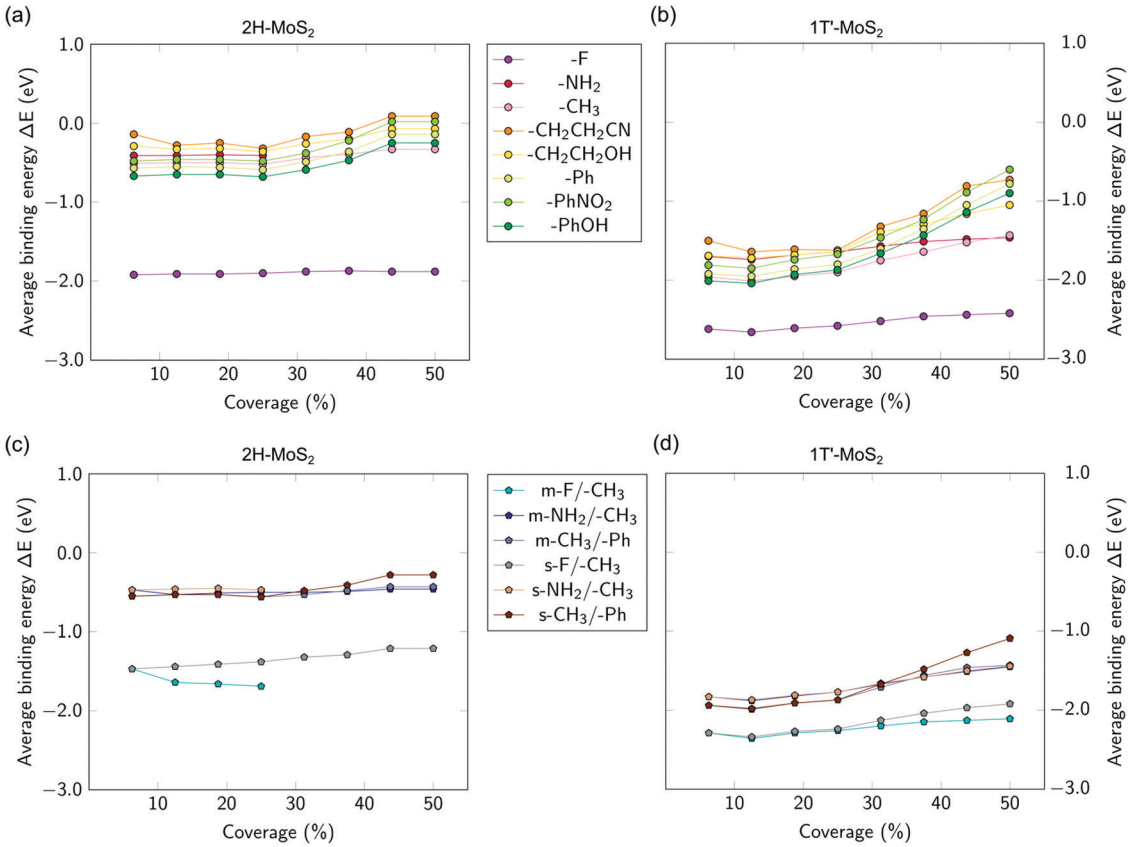

Fig. 3 Average binding energy as a function of the group coverage with respect to the 2H-MoS_2 and 1T′-MoS_2 monolayers.

of the functional group shows that when the 2H- or 1T′-MoS_2 serves as an electron-donor, the average binding energy becomes more negative for strongly electron-withdrawing groups (–F *vs.* $–NH_2$). It implies that the stronger electron-withdrawing effect could enhance the stability of the functionalized MoS_2 monolayer in this case. On the other hand, the attached groups with a stronger electron donating-ability show more negative binding energies, advocating that MoS_2 monolayers are more stable under this condition. Examples include the monofunctionalization with $–CH_2CH_2$ OH *vs.* $–CH_2CH_2$ CN or –PhOH *vs.* $–PhNO_2$.

For bisfunctionalized 2H- and 1T′-MoS_2, the average binding energy can be compared to that of the corresponding monofunctionalized case. In particular, when –F and $–CH_3$ are functionalized separately on both sides of 2H-MoS_2, the average binding energy is more negative than the average between the two corresponding monofunctionalized 2H-MoS_2. This is because the cooperative effect of electron withdrawing and donating groups could promote the charge transfer and consequently enhances its stability. Intriguingly, the average binding energy for the 1T′-MoS_2 in the case is almost equal to the monofunctionalized ones. This is attributed to the distorted octahedral structure and non-equivalent S atoms of 1T′-MoS_2, which attenuates this cooperative effect. Concerning the mixed bisfunctionalization with –F and $–CH_3$, this combined effect is offset for both 2H- and 1T′-MoS_2. As for the bisfunctionaliation of $–CH_3$ and –Ph including the separate and mixed functionalization, the average binding energy is also close to average between the two corresponding monofunctionalized MoS_2 because both of these two groups tend to donate electrons to the substrate. In summary, the investigation of the average binding energy reveals that the coverage, stereostructure and electron doping of the groups drive the stability of both functionalized 2H- and 1T′-MoS_2 monolayers.

Electronic properties

To provide a benchmark for our computational scheme, we initially apply the DFT-GW-BSE method to the bare MoS_2 monolayer. The calculated electronic band gaps with the DFT method at PBE level are 1.65 eV and 0.04 eV for 2H- and 1T′-MoS_2, respectively, whereas the self-energy correction considered in G_0W_0 method opens the band gaps to 2.51 eV and 0.08 eV, respectively. The G_0W_0 results are consistent with reported experimental values of 2.50 eV and 0.08 eV for 2H-MoS_2 and 1T′-MoS_2, respectively.[57,58] Next, we turn our attention to the functionalized 2H- and 1T′-MoS_2 monolayers. Fig. 4 depicts the variation of the electronic band gaps calculated by the G_0W_0 method with different adsorbates and coverages. The corresponding DFT results are presented in Fig. S5 (ESI†). At 6.25% coverage, the monofunctionalized and bisfunctionalized 2H-MoS_2 display semiconducting characteristics with varying QP band gaps from 0.99 eV to 2.22 eV for the considered systems.

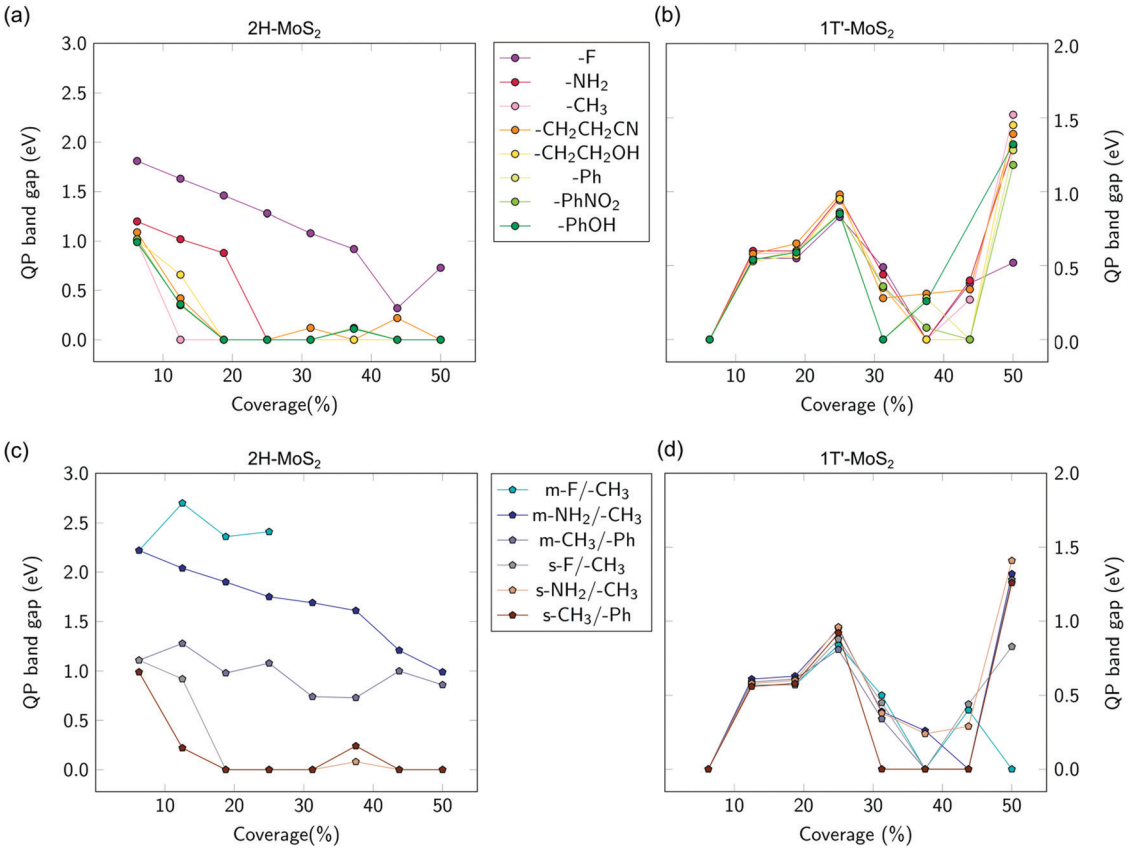

Fig. 4 QP band gaps as a function of the group coverages with respect to the functionalized 2H-MoS_2 and 1T′-MoS_2 monolayers.

The reduced band gap is associated with the donor or acceptor state inside the gap of bare 2H-MoS_2 (see Fig. S6, ESI†). The introduced state primarily originates from the Mo 4d band with additional contributions from the 3p orbitals of S and the sp orbitals of the adsorbate. This suggests that the 4d of Mo atoms will make a main contribution to the electronic transport in all cases although groups bind directly to the S atoms of MoS_2. As adsorbate coverage increases from 12.5% to 25%, the band gap tends to decrease. At even higher coverage (31.25–50%), the band gap fluctuates, except in the case of –NH_2/CH_3 and –F/CH_3. We note that the band gaps of both mono- and bisfunctionaliation are highly sensitive to the adsorption site, which is also found in other materials.[59–61] Therefore, the modification of the band gap for mixed bisfunctionalization of –NH_2/–CH_3 and –F/–CH_3 differs due to the difference in adsorption sites which arises from the intermolecular hydrogen bonds. With respect to the introduced donor or acceptor state around the Fermi level, the contribution of both S 3 p and adsorbate sp states increases with the increase of coverage for both mono- and bisfunctionalization, implying the influence of group coverage on electronic transport (Fig. S6, ESI†).

Compared with the 2H phase, the 1T′-MoS_2 exhibits different behaviors after covalent functionalization. It is obvious from Fig. 4 that at 6.25% coverage, both mono- and bisfunctionalized 1T′-MoS_2 exhibit metallic character, in contrast to 2H-MoS_2. As the coverage increases, the QP band gaps first increase and then oscillate at high coverage. Furthermore, the variation of QP band gaps of m-NH_2/–CH_3 and m-F/–CH_3 displays a similar trend as that of monofunctionalized 1T′-MoS_2. This is caused by the distorted structure of the 1T′ phase, which inhibits the formation of intermolecular hydrogen bonds and thereby enables the mixed groups to adsorb at the same or similar site with that of monofunctionalization. This also means the interaction between the adsorbate and the substrate in case of bisfunctionalized 1T′-MoS_2 is strong. Overall, our calculations reveal that the variation in the band gaps of both 2H- and 1T′-MoS_2 provides promising results of the utility of the chemical mono-/bisfunctionalization and coverages to tune the electronic properties of 2D materials.

Optical properties

Next, we examine the optical properties of the functionalized 2H- and 1T′-MoS_2, which are crucial for MoS_2-based optoelectronic devices. As a result of the low stability at high coverage, only low group coverages are considered. The corresponding optical absorption spectra of 2H phase are presented in Fig. 5. Compared to bare 2H-MoS_2, the optical absorption upon mono- and bisfunctionalization is red-shifted at 6.25% coverage. The red-shift is attributed to the interplay of two joint effects: (1) the reduced electronic band gap upon functionaliation as we discussed above and (2) the variation of the exciton binding energy (see Table S1, ESI†). Our calculation shows that at 6.25%

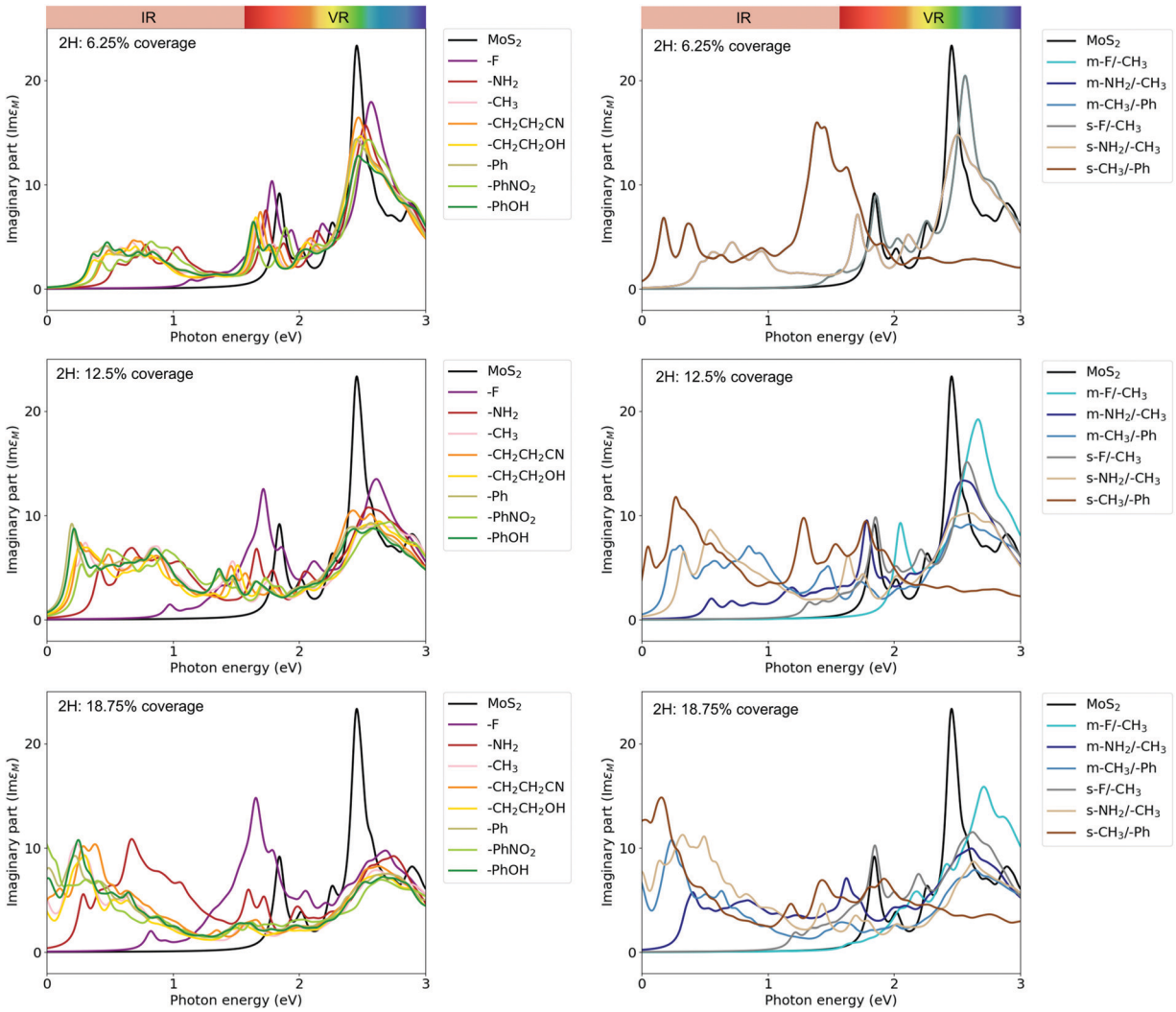

Fig. 5 Optical absorption spectra of the functionalized 2H-MoS_2 monolayer.

coverage, monofunctionalition with each group and bisfunctionalization with $-NH_2$/$-CH_3$ lowers the excitonic binding energy slightly; whereas the bisfunctionaliation with $-F$/$-CH_3$ or $-CH_3$/–Ph tends to strengthen the Coulomb interaction between the electron and hole of an exciton, promoting the formation of tight excitonic states. As the reduction of the electronic band gap is dominant upon functionalization, the optical spectrum is strongly red-shifted and the absorbance is enhanced in the 0–2 eV regime. It is worth mentioning that the optical band gap varies significantly from 0.18 eV to 1.49 eV at 6.25% coverage, indicating the high sensitivity of optical properties of 2H phase towards the different groups. As coverage increases to 18.75%, the overall optical absorbance for each functionalization remains red-shifted with a reduced optical band gap. At the same time, the intensity of the optical absorption is remarkably enhanced, especially in the spectral range of 0–1 eV.

In the case of 1T′-MoS_2, we observe an obvious blue-shift of the optical spectrum and an increase in optical absorption as the coverage increases from 6.25% to 18.75% (see Fig. S7, ESI†), which can be explained by the opening of the electronic band gap of 1T′-MoS_2 upon functionalization. Our study regarding the optical properties of the functionalized MoS_2 offers the prospect of artificially tuning the optical properties of MoS_2 by controlling the type and coverage of the functional groups.

4 Conclusion

In this work, we systemically study the stability, electronic band gap and optical absorption spectrum of both chemically functionalized 2H- and 1T′-MoS_2 for various adsorbates by means of the DFT-GW-BSE method. The chemical groups studied include –F, $-NH_2$, $-CH_3$, $-CH_2CH_2$ CN, $-CH_2CH_2$ OH, –Ph, $-PhNO_2$ and PhOH for monofunctionalization and m-F–CH_3, m-NH_2 –CH_3, m-CH_3 -Ph, s-F–CH_3, s-NH_2 –CH_3 and s-CH_3 –Ph for bisfunctionalization. We find when no intermolecular interaction is observed, the average binding energy falls at first and rises again as the coverage is elevated, reaching a minimum at 25% and 12.5% for 2H and 1T′-MoS_2, respectively. The bisfunctionalization of m-F–CH_3 and m-NH_3–CH_3 on 2H-MoS_2 can

promote the formation of intermolecular hydrogen bonds and thus improve the stability. When –F, $–NH_2$, m-F/$–CH_3$ and s-F/$–CH_3$ are attached on the surface, both of 2H- and 1T′-MoS_2 serve as electron-donors; in other cases, both of 2H- and 1T′-MoS_2 act as electron acceptors. At low coverage, the functionalized 2H-MoS_2 generally exhibits semiconducting character, whereas the functionalized 1T′-MoS_2 is predicted to be metallic; as the coverage increases, the variation of band gaps of both 2H-and 1T′-MoS_2 shows an oscillatory behavior. The changes in the electronic structure as well as the excitonic binding energy of the functionalized 2H- and 1T′-MoS_2 lead to strong modulations of their optical response with respect to the bare monolayers. In conclusion, our work demonstrates that mono- and bisfunctionalization of 2H- and 1T′-MoS_2 are vigorous tools for tuning the electronic and optical properties.

Conflicts of interest

The authors declare no conflicts of interest.

Acknowledgements

K. Wang acknowledges the China Scholarship Council for the financial support. The computations were performed with resources provided by the North-German Supercomputing Alliance (HLRN) and computer facilities of the Freie Universität Berlin (ZEDAT). Authors are also thankful to Liangliang Zhang and Jianliang Low for their assistance in the proofreading of the manuscript.

References

1 Z. Yin, H. Li, H. Li, L. Jiang, Y. Shi, Y. Sun, G. Lu, Q. Zhang, X. Chen and H. Zhang, *ACS Nano*, 2012, **6**, 74–80.
2 W. Zhang, C.-P. Chuu, J.-K. Huang, C.-H. Chen, M.-L. Tsai, Y.-H. Chang, C.-T. Liang, Y.-Z. Chen, Y.-L. Chueh, J. He-Hau, M.-Y. Chou and L.-J. Li, *Sci. Rep.*, 2014, **4**, 3826.
3 Y. Xin, X. Wang, Z. Chen, D. Weller, Y. Wang, L. Shi, X. Ma, C. Ding, W. Li, S. Guo and R. Liu, *ACS Appl. Mater. Interfaces*, 2020, **12**, 15406–15413.
4 Y. Li, H. Wang, L. Xie, Y. Liang, G. Hong and H. Dai, *J. Am. Chem. Soc.*, 2011, **133**, 7296–7299.
5 G. Li, Z. Chen, Y. Li, D. Zhang, W. Yang, Y. Liu and L. Cao, *ACS Nano*, 2020, **14**, 1707–1714.
6 H. Tabata, H. Matsuyama, T. Goto, O. Kubo and M. Katayama, *ACS Nano*, 2021, **15**, 2542–2553.
7 B. Zong, Q. Li, X. Chen, C. Liu, L. Li, J. Ruan and S. Mao, *ACS Appl. Mater. Interfaces*, 2020, **12**, 50610–50618.
8 K. Chang and W. Chen, *ACS Nano*, 2011, **5**, 4720–4728.
9 J. Xiao, D. Choi, L. Cosimbescu, P. Koech, J. Liu and J. P. Lemmon, *Chem. Mater.*, 2010, **22**, 4522–4524.
10 G. Eda and S. A. Maier, *ACS Nano*, 2013, **7**, 5660–5665.
11 M.-L. Tsai, S.-H. Su, J.-K. Chang, D.-S. Tsai, C.-H. Chen, C.-I. Wu, L.-J. Li, L.-J. Chen and J.-H. He, *ACS Nano*, 2014, **8**, 8317–8322.
12 F. Wypych and R. Schöllhorn, *J. Chem. Soc., Chem. Commun.*, 1992, 1386–1388.
13 J. A. Wilson and A. D. Yoffe, *Adv. Phys.*, 1969, **18**, 193–335.
14 I. Song, C. Park and H. C. Choi, *RSC Adv.*, 2015, **5**, 7495–7514.
15 X. Qian, J. Liu, L. Fu and J. Li, *Science*, 2014, **346**, 1344–1347.
16 R. Bissessur, M. G. Kanatzidis, J. L. Schindler and C. R. Kannewurf, *J. Chem. Soc., Chem. Commun.*, 1993, 1582–1585.
17 G. Eda, T. Fujita, H. Yamaguchi, D. Voiry, M. Chen and M. Chhowalla, *ACS Nano*, 2012, **6**, 7311–7317.
18 R. Kappera, D. Voiry, S. E. Yalcin, B. Branch, G. Gupta, A. Mohite and M. Chhowalla, *Nat. Mater.*, 2014, **13**, 1128–1134.
19 Y. Yao, K. Ao, P. Lv and Q. Wei, *Nanomaterials*, 2019, **9**, 844.
20 T. Venanzi, H. Arora, A. Erbe, A. Pashkin, S. Winnerl, M. Helm and H. Schneider, *Appl. Phys. Lett.*, 2019, **114**, 172106.
21 K. Wang and B. Paulus, *Phys. Chem. Chem. Phys.*, 2020, **22**, 11936–11942.
22 S. Mouri, Y. Miyauchi and K. Matsuda, *Nano Lett.*, 2013, **13**, 5944–5948.
23 P. Gant, P. Huang, D. Pérez de Lara, D. Guo, R. Frisenda and A. Castellanos-Gomez, *Mater. Today*, 2019, **27**, 8–13.
24 S. Wang, M. S. Ukhtary and R. Saito, *Phys. Rev. Res.*, 2020, **2**, 033340.
25 K. C. Knirsch, N. C. Berner, H. C. Nerl, C. S. Cucinotta, Z. Gholamvand, N. McEvoy, Z. Wang, I. Abramovic, P. Vecera, M. Halik, S. Sanvito, G. S. Duesberg, V. Nicolosi, F. Hauke, A. Hirsch, J. N. Coleman and C. Backes, *ACS Nano*, 2015, **9**, 6018–6030.
26 E. E. Benson, H. Zhang, S. A. Schuman, S. U. Nanayakkara, N. D. Bronstein, S. Ferrere, J. L. Blackburn and E. M. Miller, *J. Am. Chem. Soc.*, 2018, **140**, 441–450.
27 D. Voiry, A. Goswami, R. Kappera, C. d. C. C. e Silva, D. Kaplan, T. Fujita, M. Chen, T. Asefa and M. Chhowalla, *Nat. Chem.*, 2015, **7**, 45–49.
28 X. Chen, D. McAteer, C. McGuinness, I. Godwin, J. N. Coleman and A. R. McDonald, *Chem. – Eur. J.*, 2018, **24**, 351–355.
29 S. S. Chou, M. De, J. Kim, S. Byun, C. Dykstra, J. Yu, J. Huang and V. P. Dravid, *J. Am. Chem. Soc.*, 2013, **135**, 4584–4587.
30 Q. Ding, K. J. Czech, Y. Zhao, J. Zhai, R. J. Hamers, J. C. Wright and S. Jin, *ACS Appl. Mater. Interfaces*, 2017, **9**, 12734–12742.
31 S. Bertolazzi, S. Bonacchi, G. Nan, A. Pershin, D. Beljonne and P. Samorì, *Adv. Mater.*, 2017, **29**, 1606760.
32 C. Backes, N. C. Berner, X. Chen, P. Lafargue, P. LaPlace, M. Freeley, G. S. Duesberg, J. N. Coleman and A. R. McDonald, *Angew. Chem., Int. Ed.*, 2015, **54**, 2638–2642.
33 X. S. Chu, A. Yousaf, D. O. Li, A. A. Tang, A. Debnath, D. Ma, A. A. Green, E. J. G. Santos and Q. H. Wang, *Chem. Mater.*, 2018, **30**, 2112–2128.
34 I. K. Sideri, R. Arenal and N. Tagmatarchis, *ACS Mater. Lett.*, 2020, **2**, 832–837.
35 M. Vera-Hidalgo, E. Giovanelli, C. Navío and E. M. Pérez, *J. Am. Chem. Soc.*, 2019, **141**, 3767–3771.

36 X. Chen, C. Bartlam, V. Lloret, N. Moses Badlyan, S. Wolff, R. Gillen, T. Stimpel-Lindner, J. Maultzsch, G. S. Duesberg, K. C. Knirsch and A. Hirsch, *Angew. Chem., Int. Ed.*, 2021, **60**, 13484–13492.
37 E. X. Yan, M. Cabán-Acevedo, K. M. Papadantonakis, B. S. Brunschwig and N. S. Lewis, *ACS Mater. Lett.*, 2020, **2**, 133–139.
38 Q. Tang and D.-e. Jiang, *ACS Catal.*, 2016, **6**, 4953–4961.
39 Q. Tang and D.-e. Jiang, *Chem. Mater.*, 2015, **27**, 3743–3748.
40 M. Palummo, A. N. D'Auria, J. C. Grossman and G. Cicero, *J. Phys.: Condens. Matter*, 2019, **31**, 235701.
41 Y. Linghu, N. Li, Y. Du and C. Wu, *Phys. Chem. Chem. Phys.*, 2019, **21**, 9391–9398.
42 A. Gul, C. Bacaksiz, E. Unsal, B. Akbali, A. Tomak, H. M. Zareie and H. Sahin, *Mater. Res. Express*, 2018, **5**, 036415.
43 L. O. Jones, M. A. Mosquera, M. A. Ratner and G. C. Schatz, *ACS Appl. Mater. Interfaces*, 2020, **12**, 4607–4615.
44 M. S. Hybertsen and S. G. Louie, *Phys. Rev. B: Condens. Matter Mater. Phys.*, 1986, **34**, 5390–5413.
45 M. Rohlfing and S. G. Louie, *Phys. Rev. Lett.*, 1998, **81**, 2312–2315.
46 L. X. Benedict, E. L. Shirley and R. B. Bohn, *Phys. Rev. Lett.*, 1998, **80**, 4514–4517.
47 S. Albrecht, L. Reining, R. Del Sole and G. Onida, *Phys. Rev. Lett.*, 1998, **80**, 4510–4513.
48 D. Y. Qiu, F. H. da Jornada and S. G. Louie, *Phys. Rev. Lett.*, 2013, **111**, 216805.
49 L. Yang, J. Deslippe, C.-H. Park, M. L. Cohen and S. G. Louie, *Phys. Rev. Lett.*, 2009, **103**, 186802.
50 C. D. Spataru, S. Ismail-Beigi, L. X. Benedict and S. G. Louie, *Phys. Rev. Lett.*, 2004, **92**, 077402.
51 M. L. Tiago and J. R. Chelikowsky, *Solid State Commun.*, 2005, **136**, 333–337.
52 J. Enkovaara, C. Rostgaard, J. J. Mortensen, J. Chen, M. Dułak, L. Ferrighi, J. Gavnholt, C. Glinsvad, V. Haikola, H. A. Hansen, H. H. Kristoffersen, M. Kuisma, A. H. Larsen, L. Lehtovaara, M. Ljungberg, O. Lopez-Acevedo, P. G. Moses, J. Ojanen, T. Olsen, V. Petzold, N. A. Romero, J. Stausholm-Møller, M. Strange, G. A. Tritsaris, M. Vanin, M. Walter, B. Hammer, H. Häkkinen, G. K. H. Madsen, R. M. Nieminen, J. K. Nørskov, M. Puska, T. T. Rantala, J. Schiøtz, K. S. Thygesen and K. W. Jacobsen, *J. Phys.: Condens. Matter*, 2010, **22**, 253202.
53 J. P. Perdew, K. Burke and M. Ernzerhof, *Phys. Rev. Lett.*, 1996, **77**, 3865–3868.
54 W. Tang, E. Sanville and G. Henkelman, *J. Phys.: Condens. Matter*, 2009, **21**, 084204.
55 I. Tamm, in *Selected Papers*, Springer, 1991, pp. 157–174.
56 S. M. Dancoff, *Phys. Rev.*, 1950, **78**, 382–385.
57 A. R. Klots, A. K. M. Newaz, B. Wang, D. Prasai, H. Krzyzanowska, J. Lin, D. Caudel, N. J. Ghimire, J. Yan, B. L. Ivanov, K. A. Velizhanin, A. Burger, D. G. Mandrus, N. H. Tolk, S. T. Pantelides and K. I. Bolotin, *Sci. Rep.*, 2014, **4**, 6608.
58 X. Yin, Q. Wang, L. Cao, C. S. Tang, X. Luo, Y. Zheng, L. M. Wong, S. J. Wang, S. Y. Quek, W. Zhang, A. Rusydi and A. T. S. Wee, *Nat. Commun.*, 2017, **8**, 486.
59 K. Wang, J. Shao and B. Paulus, *J. Chem. Phys.*, 2021, **154**, 104705.
60 R. Nechache, C. Harnagea, L. Cardenas, W. Huang, J. Chakrabartty and F. Rosei, *Nat. Photonics*, 2015, **9**, 61–67.
61 C. Shao, C. Rui, J. Liu, T. Wang, Q. Shao and F. Chen, *Diamond Relat. Mater.*, 2020, **106**, 107824.

